

HRMedSeg: Unlocking High-resolution Medical Image segmentation via Memory-efficient Attention Modeling

Qing Xu^{1*}, Zhenye Lou^{2*}, Chenxin Li^{3*}, Xiangjian He^{1†}, Rong Qu⁴, Tesema Fiseha Berhanu¹, Yi Wang⁵, Wenting Duan⁶, and Zhen Chen⁷
¹UNNC, ²Sichuan University, ³CUHK, ⁴University of Nottingham,
⁵Dalian University of Technology, ⁶University of Lincoln, ⁷HKISI, CAS

Abstract

High-resolution segmentation is critical for precise disease diagnosis by extracting micro-imaging information from medical images. Existing transformer-based encoder-decoder frameworks have demonstrated remarkable versatility and zero-shot performance in medical segmentation. While beneficial, they usually require huge memory costs when handling large-size segmentation mask predictions, which are expensive to apply to real-world scenarios. To address this limitation, we propose a memory-efficient framework for high-resolution medical image segmentation, called HRMedSeg. Specifically, we first devise a lightweight gated vision transformer (LGViT) as our image encoder to model long-range dependencies with linear complexity. Then, we design an efficient cross-multiscale decoder (ECM-Decoder) to generate high-resolution segmentation masks. Moreover, we utilize feature distillation during pre-training to unleash the potential of our proposed model. Extensive experiments reveal that HRMedSeg outperforms state-of-the-arts in diverse high-resolution medical image segmentation tasks. In particular, HRMedSeg uses only 0.59GB GPU memory per batch during fine-tuning, demonstrating low training costs. Besides, when HRMedSeg meets the Segment Anything Model (SAM), our HRMedSegSAM takes 0.61% parameters of SAM-H. The code is available at <https://github.com/xq141839/HRMedSeg>.

1. Introduction

High-resolution medical images play a pivotal role in identifying microstructure information of tissue and organs as well as tiny lesion change from diverse modalities, e.g., Dermoscopy, Fundus, and Microscopy, advancing clinical applications in terms of precise disease diagnosis [11, 43, 67]. Moreover, mobile devices have demonstrated excep-

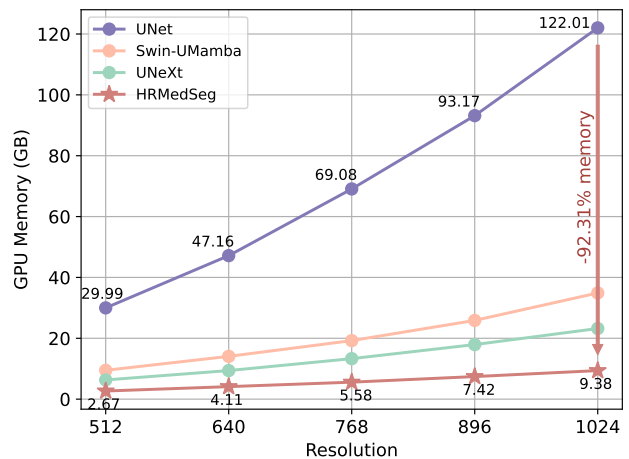


Figure 1. Comparison on training memory costs. Our HRMedSeg framework respectively reduces GPU memory costs by 92.31% and 59.59% compared to standard UNet [50] and efficient UNeXt [59] when performing a standard training setting (e.g., 16 batches) with a resolution of 1024×1024 .

tional potential in enabling fast and more accessible medical image segmentation and disease diagnosis [42, 59, 72]. Such computational resource limitations pose a significant challenge to developing high-resolution medical image segmentation frameworks with the necessary efficiency.

In the realm of medical image segmentation, existing U-shape encoder-decoder frameworks [31, 32, 50, 71, 81] with convolutional neural networks (CNNs) demonstrate superior adaptability for diverse medical segmentation tasks due to their outstanding inductive bias capabilities. These methods leverage skip connection to achieve multiscale information integration, predicting accurate segmentation masks [17, 57, 59, 63, 72]. Despite the advantage, such operations result in the rapid growth of memory consumption when dealing with high-resolution segmentation mask predictions, as illustrated in Figure 1.

Recently, Vision Transformer (ViT) [18] has revolutionized medical segmentation frameworks by modeling

*Equal contribution.

†Corresponding author: Xiangjian He (sean.he@nottingham.edu.cn).

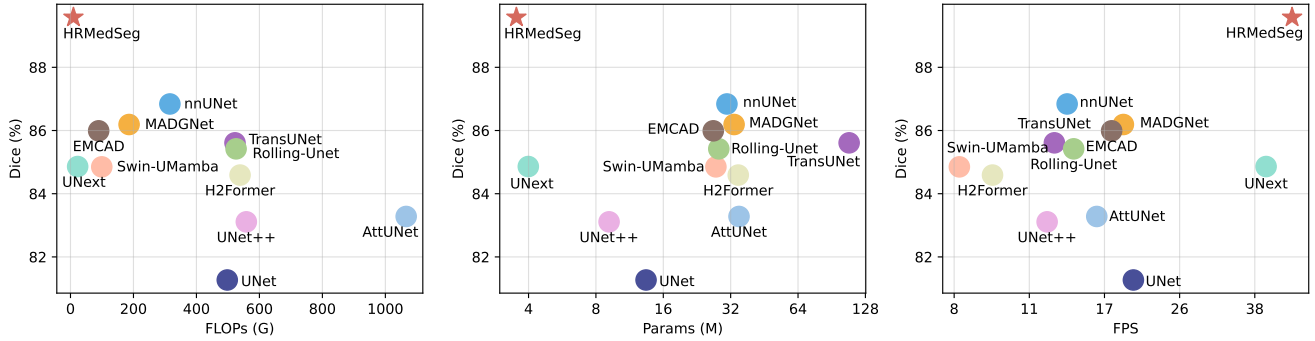


Figure 2. Efficiency comparisons between state-of-the-arts and our HRMedSeg framework. Compared to existing state-of-the-arts, our HRMedSeg demonstrates superior performance and computation efficiency.

long-range dependencies, demonstrating superior generalization capabilities across various medical imaging tasks [10, 12, 26, 78]. However, ViT-based approaches face significant computational challenges due to their inherent quadratic complexity (*i.e.*, $O(n^2)$), which becomes prohibitively expensive when processing high-resolution medical images. This computational burden severely limits their practical application in resource-constrained environments. To address this issue, some studies [30, 35, 43] have removed skip connections, but this approach sacrifices crucial multiscale learning capabilities essential for accurate medical segmentation. While linear attention mechanisms [34] offer a potential solution by reducing complexity from $O(n^2)$ to $O(n)$ through replacing the Softmax function with linear normalization, they significantly compromise feature representation power, resulting in degraded segmentation performance [14, 23]. These computational-performance tradeoffs present a critical challenge in developing efficient ViT-based medical segmentation frameworks.

To address the aforementioned limitations, we propose a memory-efficient encoder-decoder architecture for high-resolution medical image segmentation, named HRMedSeg. Specifically, we first introduce the lightweight gated vision transformer (LGViT) as our image encoder. LGViT leverages channel-interactive layers to learn low-level semantic representations and token-interactive layers to capture global contexts with linear complexity. Then, we devise the efficient cross-multiscale decoder (ECM-Decoder) that utilizes multiscale refinement of low-resolution image embeddings to eliminate the demand for pyramid decoding workflows, reducing memory costs of high-resolution segmentation mask predictions. To unleash the potential of our HRMedSeg in high-resolution medical segmentation, we adopt feature distillation based on foundation models to perform pretraining. Extensive experimental results demonstrate that our HRMedSeg performs better than state-of-the-arts in various high-resolution medical image segmentation tasks with lower memory costs. When HRMedSeg combines with the SAM series [35, 49], our HRMedSegSAM

exhibits superior zero-shot generalization capacities with efficient computation costs. The contributions are summarized as follows:

- We propose a memory-efficient HRMedSeg framework to provide an end-to-end solution for high-resolution medical image segmentation with remarkable versatility across diverse medical modalities.
- We propose an LGViT backbone as the image encoder to capture global dependencies from long-range sequences with linear computation complexity while performing sufficient expressive power.
- We devise an ECM-Decoder that leverages cross-multiscale to refine low-resolution image embedding, eliminating classical skip connections for reducing memory costs of high-resolution segmentation predictions.
- We conduct extensive experiments on diverse high-resolution medical datasets, proving that our HRMedSeg outperforms state-of-the-arts. When HRMedSeg meets SAM, our HRMedSegSAM demonstrates outstanding zero-shot segmentation performance.

2. Related Work

Medical image segmentation leverages pixel-level classification to identify and delineate regions of interest in various medical images, such as organs, lesions, and tissues within different imaging modalities (e.g., ultrasound, fundus).

The encoder-decoder architecture, UNet [50], has become a common fundamental design for many medical image segmentation models [8, 19, 20, 31, 73, 81]. To improve feature representations of the network, existing studies [1, 27, 45, 53] usually utilized attention mechanisms to highlight salient features. Particularly, Attention U-Net [51] applied spatial attention to each skip connection layer of the network to eliminate the demand for using extra disease/organ localization modules of cascaded CNNs. EMCAD [48] employed grouped channel and spatial gated attention mechanisms to efficiently catch intricate spatial relationships. However, such CNN-based frameworks suffered

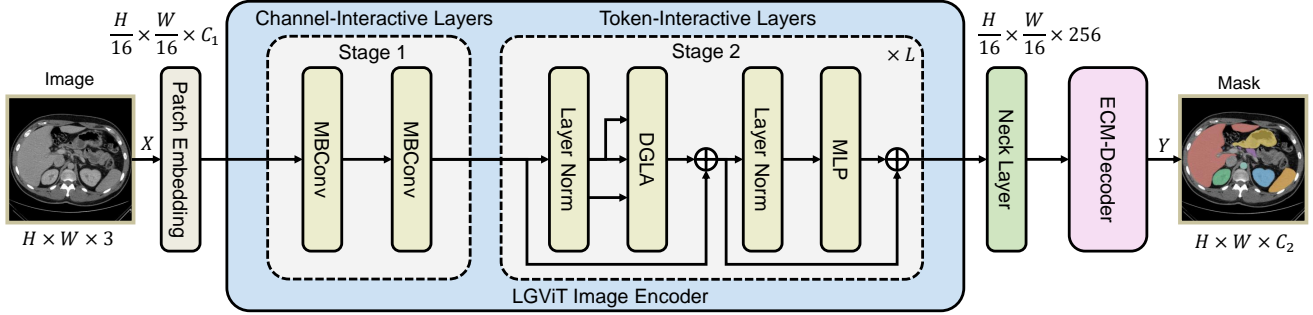


Figure 3. The overview of our memory-efficient HRMedSeg framework for high-resolution medical image segmentation.

from insufficient learning of global information due to the limited receptive field, resulting in limited generality.

ViT [18] demonstrated a superior ability to model long-range dependencies and surpassed CNN in various computer vision tasks including medical image segmentation [25, 39, 64]. Especially, Cao *et al.* [6] proposed a pure transformer-based encoder-decoder architecture that used the hierarchical Swin Transformer with shifted windows for feature extraction and segmentation decoding operations. He *et al.* [26] introduced a hyper-transformer block that combined multi-scale channel attention with self-attention to grasp local and global dependencies in medical images. The updated TransUNet [10] constructed a coarse-to-fine transformer decoder to deal with small targets like tumors. Moreover, the large model capacity of ViT enhanced its generalization capabilities to unseen domains. The recent ViT-based SAM [35] had superior performance in natural scenarios and proved its outstanding zero-shot learning ability in medical domains [7, 30, 43, 44, 66, 67]. Despite these advantages, the rapid increase in the number of parameters to ViT caused huge computational costs during training and deployment, which limited its applications in real-world scenarios. To address this issue, directly down-scaling the embedding dimensions and network layers was a common approach to decrease the model size of ViT [21, 54, 68, 70]. In addition, reducing the quadratic complexity of self-attention in ViT received widespread attention from researchers. Linear attention [34] employed linear normalization rather than the non-linear Softmax function in attention operation. Although it achieved linear complexity, previous studies [13, 23, 47] demonstrated that the insufficient expressive power of linear attention results in the degraded performance of transformer on many computer vision tasks. Mamba [22] integrated State Space Model (SSM), an advanced Recurrent Neural Network (RNN), to model long-range dependencies with linear complexity. The recent works demonstrated the effectiveness of Mamba in diverse medical image segmentation tasks [40, 69, 80]. Rather than directly integrating Mamba into the U-shape architecture, our approach adapts Mamba’s design principles to enhance the expressive power of linear attention for

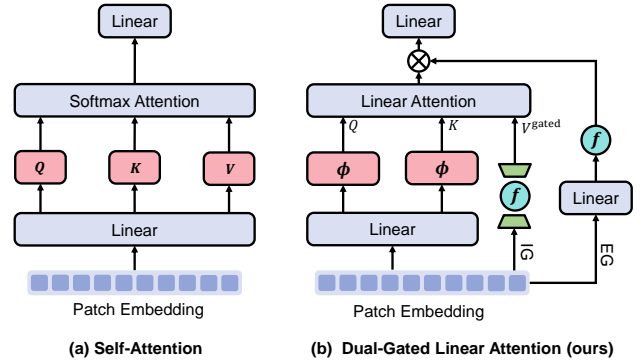


Figure 4. Difference between (a) self-attention and (b) the proposed dual-gated linear attention.

high-resolution medical image segmentation.

Furthermore, the pyramid segmentation decoding of U-shape architectures usually adopted skip connection to integrate low-level and high-level semantic information for mask generations of customized sizes [15, 31, 65, 71, 81]. Multiscale fusion was widely used to enhance the precision of predictions [17, 29, 38, 55, 63, 79]. Besides, MADGNet [45] created dual-branch decoding channels to additionally learn detailed boundary information by applying multi-task learning and deep supervision strategies. However, for high-resolution medical image segmentation, such multi-level decoding processes significantly increased memory costs. To match the constraints of mobile devices, current studies utilized depthwise convolutions [9, 24], advanced Multi-Layer Perceptrons (MLPs) [42, 59] and Kolmogorov-Arnold Networks (KANs) [37] to reduce computational costs in high-dimensional decoding layers of U-shape architectures. Different from these methods, we explore the efficiency of multi-level decoding operations and optimize the structure of the pyramid mask decoder.

3. Methodology

3.1. Overview of HRMedSeg

We present the HRMedSeg framework to provide memory-efficient high-resolution segmentation with superior perfor-

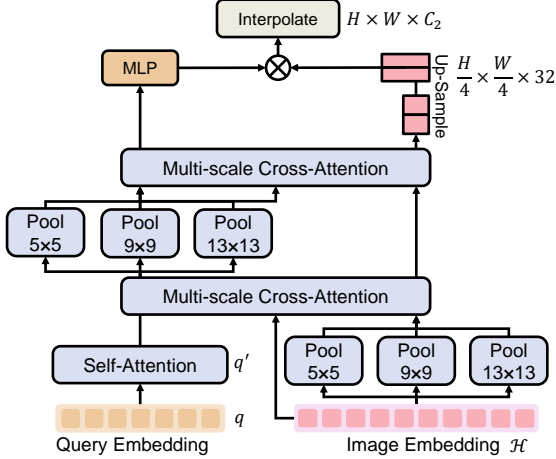


Figure 5. Architecture of our efficient cross-multiscale decoder.

mance across diverse medical imaging modalities, as illustrated in Figure 3. Our goal is to train an end-to-end model $f_\theta : X \rightarrow Y$, where θ represents learned parameters, X is the given image and Y is the predicted segmentation mask. Each pixel in this mask is assigned to a hard label based on the predefined class list. Our HRMedSeg is built upon the encoder-decoder architecture, integrating an LGViT image encoder to capture long-range dependencies with linear complexity as well as sufficient expressive power and an ECM-Decoder to generate high-resolution segmentation masks efficiently. Additionally, we leverage feature distillation during pretraining to fully realize HRMedSeg’s potential.

3.2. Lightweight Gated ViT Image Encoder

The self-attention mechanism of the standard ViT [18] brings huge computation costs when handling high-resolution medical images. Current efficient ViTs mitigate this risk by leveraging group attention [41], depthwise convolution [62], or multi-scale linear attention to decrease the number of self-attention layers. However, these methods do not take into account the efficiency of inputs. Inspired by the sparse saliency of medical images, we propose a lightweight gated vision transformer (LGViT) as the image encoder of our HRMedSeg. It is designed with a simple but memory-efficient two-stage layout, where the key idea is to improve the efficiency of attention computation and the expressive power of feature representations by eliminating redundant information inputs.

Channel-Interactive Layers. To build up our LGViT, we propose a two-stage layout that first employs two MBConvs [28] as channel-interactive layers to learn low-level representation efficiently. Specifically, each MBConv includes a 1×1 convolution $\mathcal{F}_{\text{Conv}}^{1 \times 1}$ for channel expansion. A 3×3 depthwise convolution $\mathcal{F}_{\text{DWConv}}^{3 \times 3}$ is followed by a 1×1 projection convolution $\mathcal{F}_{\text{Proj}}^{1 \times 1}$ for channel communication.

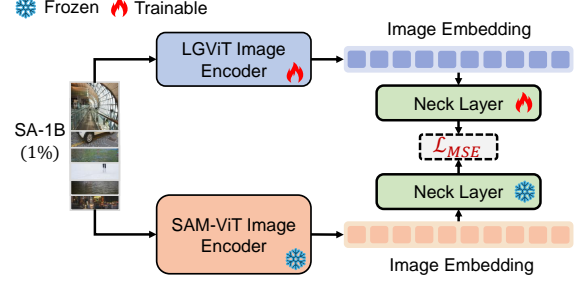


Figure 6. Pretraining feature distillation based on the image encoder of SAM [35].

Given a set of patch embeddings $x \in \mathbb{R}^{\frac{H}{S} \times \frac{W}{S} \times C_1}$, where H and W represent the height and width of the input image, respectively, S is the predefined patch size and C_1 is embedding channels, the computation can be defined by:

$$x \leftarrow \sigma(\mathcal{F}_{\text{Proj}}^{1 \times 1}(\sigma(\mathcal{F}_{\text{DWConv}}^{3 \times 3}(\sigma(\mathcal{F}_{\text{Conv}}^{1 \times 1}(x)))))) + x), \quad (1)$$

where σ stands for an activation function (e.g., GELU). On this basis, our channel-interactive layers enhance the model capability by introducing inductive bias of the local structural information.

Token-Interactive Layers. The recent Mamba [22] architectures have emerged as competitive alternatives to ViT in long-sequence visual tasks (e.g., semantic segmentation) [75]. Inspired by the success of the gating mechanism in Mamba, in the next stage, we devise the *Dual-Gated Linear Attention (DGLA)* to form token-interactive layers for learning global representations, as presented in Figure 4. Specifically, the self-attention is defined by:

$$V' = \text{softmax}\left(\frac{QK^\top}{\sqrt{d}}\right)V, \quad (2)$$

$$Q = x\mathcal{W}_Q, K = x\mathcal{W}_K, = x\mathcal{W}_V,$$

where $\mathcal{W}_Q, \mathcal{W}_K, \mathcal{W}_V \in \mathbb{R}^{C_1 \times d}$ are the learnable linear projection matrices with d representing the projection dimension. We observe that self-attention computes the similarities between all query-key pairs to update input x . This operation can be achieved by other implementations such as the gating mechanism. Therefore, our dual-gated linear attention rewrites Equation 2 to:

$$V'_i = \sum_{j=1}^N \frac{\phi(Q_i)\phi(K_j)^\top}{\sum_{j=1}^N \phi(Q_i)\phi(K_j)^\top} V_j^{\text{gated}}, \quad (3)$$

where V_i represents the i -th row of matrix V , ϕ is the kernel function following [34], $N = H \times W/S$ and V^{gated} is obtained by a inter-gated (IG) network:

$$V^{\text{gated}} = f(V)\mathcal{W}_{\text{gate}}, \quad (4)$$

where $\mathcal{W}_{\text{gate}} \in \mathbb{R}^{d \times C_1}$ and $f(\cdot)$ is the SiLU function. The inter-gated network leverages the nonlinear transformations

Table 1. Comparison with state-of-the-arts on 2D medical image segmentation. #Mem and #FLOPs of all methods are reported based on the 1024×1024 input.

Methods	#Mem	#FLOPs	#Params	Dermoscopy		X-ray		Fundus		Ultrasound		Microscopy	
				Dice	mIoU								
U-Net [50]	7.63GB	497.91G	13.40M	80.36	70.23	96.30	92.94	86.86	77.72	69.66	57.61	87.52	80.39
U-Net++ [79]	9.82GB	558.46G	9.16M	82.06	72.95	96.43	93.18	88.49	79.92	70.66	58.83	88.97	82.67
AttUNet [51]	12.18GB	1066.11G	34.87M	82.40	73.42	96.19	92.74	89.04	80.67	72.06	60.12	89.03	82.81
nnUNet [32]	7.15GB	315.70G	30.80M	85.08	76.74	<u>96.74</u>	<u>93.78</u>	89.13	80.76	<u>77.07</u>	<u>70.08</u>	90.48	82.89
UNext [59]	<u>1.45G</u>	<u>22.75GB</u>	<u>3.99M</u>	85.27	77.36	96.42	93.27	86.14	76.31	76.45	66.82	90.16	82.63
TransUNet [10]	15.69GB	522.45G	108.27M	86.44	78.89	96.56	93.42	88.43	79.80	72.18	60.85	91.12	84.31
H2Former [26]	37.37GB	538.58G	34.60M	85.20	77.33	96.45	93.23	89.22	81.09	72.02	60.05	90.79	83.86
Swin-UMamba [40]	2.18GB	99.35G	27.49M	85.34	76.64	96.72	93.74	87.93	78.69	70.72	58.97	90.04	82.59
Rolling-Unet [40]	8.30GB	525.93G	28.32M	85.13	77.03	96.63	93.51	88.19	79.39	73.24	62.06	90.93	83.98
MADGNet [45]	3.18GB	186.11G	33.15M	85.96	77.95	96.55	93.40	88.65	80.09	73.91	62.62	<u>91.20</u>	84.49
EMCAD [48]	4.03GB	89.53G	26.76M	<u>86.97</u>	<u>79.52</u>	96.74	93.77	<u>89.44</u>	<u>81.31</u>	73.13	61.74	90.62	83.76
HRMedSeg	0.59GB	9.39G	3.53M	88.63	81.62	96.86	94.00	89.81	81.84	85.50	77.30	92.10	85.78

Table 2. Comparison with state-of-the-arts on 3D medical image segmentation.

Methods	Average			Aorta	Gallbladder	Kidney (L)	Liver	Pancreas	Spleen	Stomach	Kidney (R)
	Dice	mIoU	HD								
U-Net [50]	74.17	68.06	98.39	86.24	58.79	81.83	88.96	49.31	81.57	66.50	80.17
U-Net++ [79]	78.11	71.25	64.44	91.82	66.57	88.33	92.42	50.08	85.13	65.91	84.65
AttUNet [51]	78.16	71.21	63.78	91.41	60.52	85.61	91.81	53.06	86.71	70.44	85.71
nnUNet [32]	81.48	74.79	49.57	<u>92.33</u>	65.08	87.52	92.55	60.28	90.89	77.35	<u>85.87</u>
UNext [59]	79.27	72.03	51.57	90.38	65.66	87.25	90.83	58.54	87.47	70.49	83.53
TransUNet [10]	81.31	74.15	53.22	91.37	67.84	88.26	89.79	64.05	89.51	76.13	83.55
H2Former [26]	78.32	70.83	52.04	90.80	64.19	87.94	90.91	51.93	87.63	70.60	82.59
Swin-UMamba [40]	76.71	69.14	54.66	90.37	60.76	87.22	89.55	51.10	85.85	67.41	81.44
Rolling-Unet [42]	80.75	73.61	50.32	90.63	67.25	86.98	90.24	60.16	89.82	77.32	83.56
MADGNet [45]	81.37	74.43	50.76	91.87	68.19	87.34	91.31	59.58	<u>91.38</u>	75.88	85.40
EMCAD [48]	<u>83.24</u>	<u>76.45</u>	<u>43.31</u>	91.95	<u>69.59</u>	<u>90.79</u>	<u>92.60</u>	<u>65.47</u>	91.53	79.95	84.03
HRMedSeg	84.25	77.57	36.09	92.58	72.33	91.46	93.75	70.06	89.08	<u>78.59</u>	86.17

to improve the efficiency of *value* representation. Further, we apply an exter-gated (EG) network to our dual-gated linear attention for discerning the utility of x . The final image embedding \mathcal{H} can be calculated by:

$$\mathcal{H} = \mathcal{F}_{MLP}(\mathcal{F}_{LN}(f(x\mathcal{W}_x)V')) + x, \quad (5)$$

where $\mathcal{H} \in \mathbb{R}^{N \times C_1}$, $\mathcal{W}_x \in \mathbb{R}^{C_1 \times d}$, $\mathcal{F}_{MLP}(\cdot)$ is MLP and $\mathcal{F}_{LN}(\cdot)$ is LayerNorm. Overall, the proposed LGViT adopts channel-interactive to learn low-level representations efficiently and token-interactive layers to capture long-range visual dependencies with linear complexity and perform efficient attention computations.

3.3. Efficient Cross-Multiscale Decoder

The traditional U-shape architectures utilize skip connections and pyramid decoding operations to recover mask sizes. However, such structures are computationally costly for high-resolution medical image segmentation. To address this issue, we devise an efficient cross-multiscale decoder (ECM-Decoder) that adds multiscale decoding information in high-dimension but small-size image embeddings

to eliminate the demand for pyramid decoding. As shown in Figure 5, we first create query embeddings $q \in \mathbb{R}^{C_2 \times 256}$ to learn the decoding information, where C_2 is the number of prediction categories. Then, we apply self-attention $\mathcal{F}_{SA}(\cdot)$ to update the mask query: $q' = \mathcal{F}_{SA}(q)$, followed by the bidirectional multiscale cross-attention layers with q' to update the image embedding. The above operations can be formulated as:

$$q' \leftarrow \text{softmax}\left(\frac{q'(\mathcal{H} + \psi)^\top}{\sqrt{d}}\right)\delta(\mathcal{H}) + q', \quad (6)$$

$$\mathcal{H} \leftarrow \text{softmax}\left(\frac{(\delta(\mathcal{H}) + \psi)(q')^\top}{\sqrt{d}}\right)q' + \delta(\mathcal{H}), \quad (7)$$

where ψ is the positional encoding for enhancing the dependence between geometric location and type and $\delta(\cdot)$ represents a multiscale module, which includes three parallel pooling operators [76] of different kernel sizes to enhance semantic information at diverse scales without extra parameters. Finally, the generation of segmentation masks Y can

Table 3. Comparison on medical video segmentation.

Methods	CVC-ColonDB		CVC-ClinicDB	
	Dice	mIoU	Dice	mIoU
U-Net [50]	69.27	61.84	86.02	78.07
U-Net++ [79]	71.14	62.03	88.98	82.24
AttUNet [51]	72.50	63.20	86.85	78.50
nnUNet [32]	<u>83.67</u>	<u>76.28</u>	91.06	85.02
UNext [59]	76.63	69.27	88.52	81.46
TransUNet [10]	79.54	71.06	89.27	82.98
H2Former [26]	76.08	65.89	88.63	81.71
Swin-UMamba [40]	80.61	72.72	90.73	84.81
Rolling-Unet [42]	78.29	70.25	90.21	83.97
MADGNet [45]	80.79	72.93	91.10	85.08
EMCAD [48]	76.65	69.41	<u>91.16</u>	<u>85.55</u>
HRMedSeg	85.03	78.21	94.42	89.79

be defined by:

$$Y = \text{sigmoid}(\mathcal{F}_{\text{inter}}(\mathcal{F}_{\text{trans}}(\mathcal{H}) \cdot \mathcal{F}_{\text{MLP}}(q'))), \quad (8)$$

where $Y \in \mathbb{R}^{H \times W \times C_2}$, $\mathcal{F}_{\text{trans}}(\cdot)$ stands for two transpose convolutions and $\mathcal{F}_{\text{inter}}(\cdot)$ is a bilinear interpolation function that recovers the mask sizes directly. As a result, the proposed ECM-Decoder eliminates the demand for pyramid decoding, reducing computation costs in high-resolution medical image segmentation tasks.

3.4. Pretraining Feature Distillation

Pretraining is crucial for unlocking a network’s full potential in downstream tasks. Recent studies [77] have shown that directly pretraining small models on large-scale data yields limited benefits. To enhance the quality of feature representations generated by the image encoder, which is critical for effective segmentation decoding, we implement a straightforward feature distillation approach to pretrain the LGViT component of HRMedSeg, as illustrated in Figure 6. The recent SAM [35] has shown superior performance in natural scenarios as it was trained on massive data. To take this advantage, we select the image encoder of SAM-H as the distillation target. Specifically, we connect a neck layer to our LGViT to align the feature dimension with the image encoder of SAM. The neck layer is composed of a 1×1 convolution followed by a 3×3 convolution. We optimize the distillation process using Mean Squared Error (MSE) loss on 1% samples of the SA-1B dataset [35].

3.5. Memory-Efficient Architecture

The expansion ratio in MLP is generally set to 4 in the original ViT, which makes the hidden dimension $4 \times$ wider than the embedding dimension C_1 . Despite this setting improving model capacity, the wider dimension consumes a significant portion of the memory resource. To mitigate this bottleneck, the proposed HRMedSeg sets the expansion ratio as 2 in both MBConvs and MLP following the insights of the

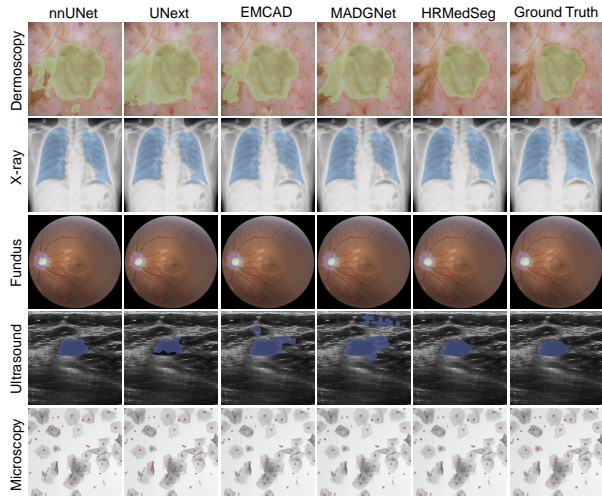


Figure 7. Qualitative results of 2D medical image segmentation.

recent studies [3, 62, 70]. In addition, the width of the embedding dimension C_1 and the depth L of the network are also major factors that affect memory costs. The previous study [68] has proven that the wider dimension facilitates the learning of hard-sample representations during training whereas feature distillation can avoid the drawbacks of hard samples since it eliminates the demand for using ground truth labels. Moreover, the deeper model is more likely to lead to overfitting on medical datasets as they usually contain limited fully-annotated labels due to the expensive costs of pixel-level annotations. Therefore, our HRMedSeg adopts a narrower embedding dimension and shallow structure (*i.e.*, $C_1 = 96$, $L = 10$).

4. Experiments

In this section, we first provide a brief introduction of our selected datasets and implementation details. Then, we illustrate the evaluation and ablation experimental results. Due to the page limit, we present the detailed dataset description in the supplementary material.

4.1. Datasets

To comprehensively validate the effectiveness of our proposed HRMedSeg framework, we first conduct the evaluation on five high-resolution 2D medical image datasets with different modalities, including Dermoscopy (2304×3072) [16, 58], X-ray (4020×4892) [5, 33], Fundus (2124×2056) [46], Ultrasound (760×570) [74] and Microscopy (1024×1024) [4]. Secondly, we evaluate our model on various organs (512×512) [36] for 3D medical image segmentation. Finally, we conduct experiments on medical video segmentation with two different Colonoscopy datasets (884×1280) [2, 56, 60]. To quantify performance on 2D and video segmentations, we select two metrics, Dice

Table 4. Comparison with state-of-the-arts on zero-shot generalization capabilities. All frameworks are distilled from SAM-H on 1% samples of the SA-1B dataset [35] and evaluated on all samples of each dataset with the box prompt mode.

Methods	#Params (Backbone)	#FLOPs (Backbone)	2D		3D		Video	
			Dice	mIoU	Dice	HD	Dice	mIoU
SAM-H [35]	637.03M	2733.64G	84.19	74.59	89.65	25.86	91.19	84.68
TinySAM [52]	6.07M	36.74G	78.45	65.17	75.38	51.70	70.28	56.80
MobileSAM [77]	6.07M	36.74G	81.73	71.69	88.76	30.39	89.92	82.89
RepViT-SAM [62]	5.12M	18.61G	81.84	71.83	88.83	29.79	90.09	83.06
EfficientSAM [70]	6.16M	25.04G	81.34	70.80	79.39	42.38	83.37	72.31
HRMedSegSAM	1.57M	6.43G	<u>81.98</u>	<u>71.97</u>	<u>88.92</u>	<u>28.15</u>	<u>90.17</u>	<u>83.26</u>
SAM2-L [49]	212.70M	810.99G	86.76	78.03	92.23	20.38	92.88	87.06
HRMedSegSAM2	1.57M	6.43G	85.13	75.61	89.54	26.89	90.47	83.68

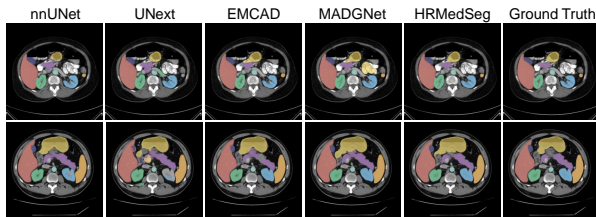


Figure 8. Qualitative results of 3D multi-organ segmentation.

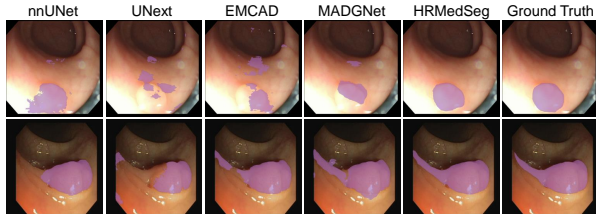


Figure 9. Qualitative results of medical video segmentation.

and mIoU, which are widely used in medical image segmentation [9, 26, 42, 43, 59]. For the 3D medical image segmentation, we adopt common evaluation metrics of existing studies [10, 48, 69].

4.2. Implementation Details

We perform all experiments on a NVIDIA A6000 GPU with PyTorch. We adopt the optimizer using Adam with a learning rate of 1×10^{-4} and apply the exponential decay strategy to adjust the learning rate, where the factor is set as 0.98. The batch size and epochs are set to 16 and 200, respectively. All images are resized to 1024×1024 during the fine-tuning and evaluation stages. The combination of Dice and focal loss functions [30, 35, 67] is used to optimize models. For fair comparison, the encoder of all baselines is pretrained using our feature distillation method. To implement zero-shot evaluation, we combine the unfine-tuned pretrained encoder of HRMedSeg with the prompt encoder and mask decoder of the SAM family.

4.3. Comprehensive Comparison Results

We compare our HRMedSeg with 11 advanced medical image segmentation models based on CNN [32, 45, 48, 50, 51, 79], ViT [10, 26], Mamba [40] and lightweight architectures [42, 59]. All models are reimplemented using the same training setting. The best and second-best performance values are highlighted in **bold** and underlined.

2D Medical Image Segmentation. As shown in Table 1, UNext [59] and DCSAU-Net [72] cost small number of parameters but are inferior to nnUNet [32], MADGNet [45] or EMCAD [48]. In contrast, our HRMedSeg framework outperforms state-of-the-arts in all five 2D medical segmentation datasets across different modalities. Especially, HRMedSeg reduces the GPU memory usage by 59.31%, 91.75%, 81.45% and 85.36% compared to UNext [59], nnUNet [32], MADGNet [45] and EMCAD [48].

3D Medical Image Segmentation. Table 2 reveals the experimental result in the 3D multi-organ segmentation dataset [36]. We report the Dice score for individual organ evaluation. It can be demonstrated that the proposed HRMedSeg surpasses the second-ranked EMCAD [48] in most organ segmentation tasks, with an average Dice and mIoU improvement of 1.01% and 1.12%. In particular, HRMedSeg achieves the lowest Hausdorff Distance (HD) of 36.09, indicating superior boundary localization.

Medical Video Segmentation. Table 3 indicates that our HRMedSeg performs better than all state-of-the-art methods in two polyp segmentation datasets. Compared with nnUNet [32] and EMCAD [48], HRMedSeg achieves a significant Dice score increase of 1.36% and 3.26% in CVC-ColonDB and CVC-ClinicDB [60], respectively. As a result, the proposed HRMedSeg achieves the new state-of-the-art results in various medical segmentation tasks and demonstrates lower computational costs.

Zero-shot Generalization. We further combine the unfine-tuned pretrained LGViT with the prompt encoder and mask decoder of SAM [35] and SAM2 [49]. Table 4 exhibits the

Table 5. Ablation study of our HRMedSeg. *E*: LGViT; *D*: ECM-Decoder; *P*: Pretraining Feature Distillation.

<i>E</i>	<i>D</i>	<i>P</i>	#Mem	#FLOPs	#Params	Dice
			7.63GB	497.71G	13.84M	77.12
✓			2.57GB	97.41G	5.59M	82.76
✓	✓		0.59GB	9.39G	3.53M	86.61
✓	✓	✓	0.59GB	9.39G	3.53M	88.63

Table 6. Analysis of depth *L* and embedding width *C* in LGViT.

<i>L</i>	<i>C</i>	#Mem	#FLOPs	#Params	Dice
4	96	0.45GB	7.43G	3.04M	87.82
8	96	0.51GB	8.74G	3.37M	88.36
12	96	0.71GB	10.05G	3.69M	88.69
16	96	0.88GB	11.36G	4.01M	88.74
10	24	0.38GB	5.73G	2.63M	85.59
10	48	0.46GB	6.52G	2.82M	87.84
10	192	0.95GB	20.43G	6.22M	88.98
10	384	1.67GB	63.56G	16.75M	89.15
10	96	0.59GB	9.39G	3.53M	88.63

Table 7. Ablation study of two-stage layout design in LGViT.

LGViT	#Mem	#FLOPs	#Params	Dice
w/o channel-interactive layers	0.55GB	9.06G	3.45M	85.39
w/o token-interactive layers	0.32GB	6.12G	2.72M	76.13
Full	0.59GB	9.39G	3.53M	88.63

average zero-shot performance in all eight medical datasets with the box prompt mode. It can be observed that the proposed LGViT of HRMedSegSAM achieves lower parameter costs and computation complexity compared with the backbone of lightweight SAMs (*e.g.*, RepViT-SAM [61], EfficientSAM [70]), displaying superior generalization performance in diverse medical modalities when combined with SAM2 [49], *i.e.*, HRMedSegSAM2.

4.4. Ablation Study

In this section, we conduct comprehensive ablation studies on the Dermoscopy dataset [16, 58] to investigate the effectiveness of our each module in HRMedSeg. As shown in Table 5, we consider the original UNet framework [50] as the ablation baseline. By introducing the LGViT, the performance is improved with the Dice of all datasets gain of 5.64%, while GPU memory usage, FLOPs, and the number of parameters are reduced by 2.97 \times , 5.11 \times and 2.48 \times . Moreover, we explore the effect of combined LGViT and ECM-Decoder, resulting in a significant Dice score increase of 3.85% and further decreasing computation costs. The pretraining feature distillation method enables our HRMedSeg to obtain additional performance improvements.

The Significance of Components in LGViT. In addition, we provide the hyperparameter investigation of LGViT in

Table 8. Ablation study of DGLA in LGViT.

Inter-Gate	Exter-Gate	#Mem	#FLOPs	#Params	Dice
✓		0.51GB	8.76G	3.39M	86.17
	✓	0.65GB	10.73G	3.92M	84.63
✓	✓	0.59GB	9.39G	3.53M	88.63

Table 9. Analysis of multiscale fusion in ECM-Decoder.

Pool 5 \times 5	Pool 9 \times 9	Pool 13 \times 13	FPS	Dice
			41.46	86.96
✓			41.29	87.54
✓	✓		41.13	88.21
✓	✓	✓	40.87	88.63

Table 6. It can be observed that the deeper network structure brings limited performance gains. On the other hand, the wider embedding dimension remarkably raises the memory costs, model complexity, and number of parameters with a slight performance improvement. Further, we comprehensively analyze the effectiveness of channel-interactive and token-interactive layers in LGViT, as presented in Table 7. We observe that removing each component rapidly drops the Dice score of HRMedSeg, which is an unworthy deal to acquire higher computation efficiency. Table 8 reveals the importance of cooperating inter-gate and exter-gate modules in token-interactive layers. In this way, the proposed LGViT with the appropriate design presents remarkable performance-efficiency trade-offs.

The Effectiveness of ECM-Decoder. Furthermore, as illustrated in Table 5, our proposed ECM-Decoder reduces GPU memory usage, FLOPs, and the number of parameters by 4.36 \times , 10.37 \times , and 1.58 \times while achieving a significant Dice score improvement of 3.85% compared to the classical U-shape decoder. Table 9 shows that by separately adding Pool 5 \times 5, Pool 9 \times 9 and Pool 13 \times 13 operators, the performance of our HRMedSeg is improved with a slight FPS decrease, maintaining the efficiency. These comparisons demonstrate the high memory efficiency of our ECM-Decoder in high-resolution medical image segmentation.

5. Conclusion

In this paper, we propose a memory-efficient HRMedSeg framework for high-resolution medical image segmentation. Specifically, the LGViT is introduced to capture global contexts with linear complexity and perform sufficient expressive power. Then, the ECM-Decoder is devised to eliminate the requirement of pyramid decoding, significantly reducing memory usage. Moreover, we adopt pretraining feature distillation to unleash the potential of HRMedSeg. Extensive experiments demonstrate that HRMedSeg outperforms state-of-the-arts with efficient computational costs in high-resolution medical segmentation.

References

- [1] Md Shariful Alam, Dadong Wang, Qiyu Liao, and Arcot Sowmya. A multi-scale context aware attention model for medical image segmentation. *IEEE Journal of Biomedical and Health Informatics*, 27(8):3731–3739, 2022. 2
- [2] Jorge Bernal, F Javier Sánchez, Gloria Fernández-Esparrach, Debra Gil, Cristina Rodríguez, and Fernando Vilarinho. Wm-dova maps for accurate polyp highlighting in colonoscopy: Validation vs. saliency maps from physicians. *Computerized medical imaging and graphics*, 43:99–111, 2015. 6
- [3] Han Cai, Junyan Li, Muyan Hu, Chuang Gan, and Song Han. Efficientvit: Lightweight multi-scale attention for high-resolution dense prediction. In *Proceedings of the IEEE/CVF International Conference on Computer Vision*, pages 17302–17313, 2023. 6
- [4] Juan C Caicedo, Allen Goodman, Kyle W Karhohs, Beth A Cimini, Jeanelle Ackerman, Marzieh Haghighi, CherKeng Heng, Tim Becker, Minh Doan, Claire McQuin, et al. Nucleus segmentation across imaging experiments: the 2018 data science bowl. *Nature Methods*, 16(12):1247–1253, 2019. 6
- [5] Sema Candemir, Stefan Jaeger, Kannappan Palaniappan, Jonathan P Musco, Rahul K Singh, Zhiyun Xue, Alexandros Karargyris, Sameer Antani, George Thoma, and Clement J McDonald. Lung segmentation in chest radiographs using anatomical atlases with nonrigid registration. *IEEE transactions on medical imaging*, 33(2):577–590, 2013. 6
- [6] Hu Cao, Yueyue Wang, Joy Chen, Dongsheng Jiang, Xiaopeng Zhang, Qi Tian, and Manning Wang. Swin-unet: Unet-like pure transformer for medical image segmentation. In *European conference on computer vision*, pages 205–218. Springer, 2022. 3
- [7] Cheng Chen, Juzheng Miao, Dufan Wu, Aoxiao Zhong, Zhiling Yan, Sekeun Kim, Jiang Hu, Zhengliang Liu, Lichao Sun, Xiang Li, et al. Ma-sam: Modality-agnostic sam adaptation for 3d medical image segmentation. *Medical Image Analysis*, 98:103310, 2024. 3
- [8] Gongping Chen, Lei Li, Yu Dai, Jianxun Zhang, and Moi Hoon Yap. Aau-net: an adaptive attention u-net for breast lesions segmentation in ultrasound images. *IEEE Transactions on Medical Imaging*, 42(5):1289–1300, 2022. 2
- [9] Junren Chen, Rui Chen, Wei Wang, Junlong Cheng, Lei Zhang, and Liangyin Chen. Tinyu-net: Lighter yet better u-net with cascaded multi-receptive fields. In *International Conference on Medical Image Computing and Computer-Assisted Intervention*, pages 626–635. Springer, 2024. 3, 7
- [10] Jieneng Chen, Jieru Mei, Xianhang Li, Yongyi Lu, Qihang Yu, Qingyue Wei, Xiangde Luo, Yutong Xie, Ehsan Adeli, Yan Wang, et al. Transunet: Rethinking the u-net architecture design for medical image segmentation through the lens of transformers. *Medical Image Analysis*, 97:103280, 2024. 2, 3, 5, 6, 7
- [11] Xuxin Chen, Ximin Wang, Ke Zhang, Kar-Ming Fung, Theresa C Thai, Kathleen Moore, Robert S Mannel, Hong Liu, Bin Zheng, and Yuchen Qiu. Recent advances and clinical applications of deep learning in medical image analysis. *Medical image analysis*, 79:102444, 2022. 1
- [12] Bowen Cheng, Ishan Misra, Alexander G Schwing, Alexander Kirillov, and Rohit Girdhar. Masked-attention mask transformer for universal image segmentation. In *Proceedings of the IEEE/CVF conference on computer vision and pattern recognition*, pages 1290–1299, 2022. 2
- [13] Krzysztof Marcin Choromanski, Valerii Likhoshesterov, David Dohan, Xingyou Song, Andreea Gane, Tamas Sarlos, Peter Hawkins, Jared Quincy Davis, Afroz Mohiuddin, Lukasz Kaiser, et al. Rethinking attention with performers. In *International Conference on Learning Representations*, 2020. 3
- [14] Krzysztof Marcin Choromanski, Valerii Likhoshesterov, David Dohan, Xingyou Song, Andreea Gane, Tamas Sarlos, Peter Hawkins, Jared Quincy Davis, Afroz Mohiuddin, Lukasz Kaiser, David Benjamin Belanger, Lucy J Colwell, and Adrian Weller. Rethinking attention with performers. In *International Conference on Learning Representations*, 2021. 2
- [15] G Jignesh Chowdary and Zhaozheng Yin. Diffusion transformer u-net for medical image segmentation. In *International conference on medical image computing and computer-assisted intervention*, pages 622–631. Springer, 2023. 3
- [16] Noel Codella, Veronica Rotemberg, Philipp Tschandl, M Emre Celebi, Stephen Dusza, David Gutman, Brian Helba, Aadi Kalloo, Konstantinos Liopyris, Michael Marchetti, et al. Skin lesion analysis toward melanoma detection 2018: A challenge hosted by the international skin imaging collaboration (isic). *arXiv preprint arXiv:1902.03368*, 2019. 6, 8
- [17] Duwei Dai, Caixia Dong, Qingsen Yan, Yongheng Sun, Chunyan Zhang, Zongfang Li, and Songhua Xu. I2u-net: A dual-path u-net with rich information interaction for medical image segmentation. *Medical Image Analysis*, page 103241, 2024. 1, 3
- [18] Alexey Dosovitskiy, Lucas Beyer, Alexander Kolesnikov, Dirk Weissenborn, Xiaohua Zhai, Thomas Unterthiner, Mostafa Dehghani, Matthias Minderer, Georg Heigold, Sylvain Gelly, Jakob Uszkoreit, and Neil Houlsby. An image is worth 16x16 words: Transformers for image recognition at scale. In *International Conference on Learning Representations*, 2021. 1, 3, 4
- [19] Deng-Ping Fan, Ge-Peng Ji, Tao Zhou, Geng Chen, Huazhu Fu, Jianbing Shen, and Ling Shao. Pranel: Parallel reverse attention network for polyp segmentation. In *International conference on medical image computing and computer-assisted intervention*, pages 263–273. Springer, 2020. 2
- [20] Deng-Ping Fan, Tao Zhou, Ge-Peng Ji, Yi Zhou, Geng Chen, Huazhu Fu, Jianbing Shen, and Ling Shao. Inf-net: Automatic covid-19 lung infection segmentation from ct images. *IEEE transactions on medical imaging*, 39(8):2626–2637, 2020. 2
- [21] Jianhai Fu, Yuanjie Yu, Ningchuan Li, Yi Zhang, Qichao Chen, Jianping Xiong, Jun Yin, and Zhiyu Xiang. Lite-sam

- is actually what you need for segment everything. *European conference on computer vision*, 2024. 3
- [22] Albert Gu and Tri Dao. Mamba: Linear-time sequence modeling with selective state spaces. *arXiv preprint arXiv:2312.00752*, 2023. 3, 4
- [23] Dongchen Han, Xuran Pan, Yizeng Han, Shiji Song, and Gao Huang. Flatten transformer: Vision transformer using focused linear attention. In *Proceedings of the IEEE/CVF international conference on computer vision*, pages 5961–5971, 2023. 2, 3
- [24] Zhaoquan Hao, Hongyan Quan, and Yinbin Lu. Emf-former: An efficient and memory-friendly transformer for medical image segmentation. In *International Conference on Medical Image Computing and Computer-Assisted Intervention*, pages 231–241. Springer, 2024. 3
- [25] Ali Hatamizadeh, Yucheng Tang, Vishwesh Nath, Dong Yang, Andriy Myronenko, Bennett Landman, Holger R Roth, and Daguang Xu. Unetr: Transformers for 3d medical image segmentation. In *Proceedings of the IEEE/CVF winter conference on applications of computer vision*, pages 574–584, 2022. 3
- [26] Along He, Kai Wang, Tao Li, Chengkun Du, Shuang Xia, and Huazhu Fu. H2former: An efficient hierarchical hybrid transformer for medical image segmentation. *IEEE Transactions on Medical Imaging*, 42(9):2763–2775, 2023. 2, 3, 5, 6, 7
- [27] Moein Heidari, Amirhossein Kazerouni, Milad Soltany, Reza Azad, Ehsan Khodapanah Aghdam, Julien Cohen-Adad, and Dorit Merhof. Hiformer: Hierarchical multi-scale representations using transformers for medical image segmentation. In *Proceedings of the IEEE/CVF winter conference on applications of computer vision*, pages 6202–6212, 2023. 2
- [28] Andrew Howard, Mark Sandler, Grace Chu, Liang-Chieh Chen, Bo Chen, Mingxing Tan, Weijun Wang, Yukun Zhu, Ruoming Pang, Vijay Vasudevan, et al. Searching for mobilenetv3. In *Proceedings of the IEEE/CVF international conference on computer vision*, pages 1314–1324, 2019. 4
- [29] Huimin Huang, Lanfen Lin, Ruofeng Tong, Hongjie Hu, Qiaowei Zhang, Yutaro Iwamoto, Xianhua Han, Yen-Wei Chen, and Jian Wu. Unet 3+: A full-scale connected unet for medical image segmentation. In *ICASSP 2020-2020 IEEE international conference on acoustics, speech and signal processing (ICASSP)*, pages 1055–1059. IEEE, 2020. 3
- [30] Yuhao Huang, Xin Yang, Lian Liu, Han Zhou, Ao Chang, Xinrui Zhou, Rusi Chen, Junxuan Yu, Jiongquan Chen, Chaoyu Chen, et al. Segment anything model for medical images? *Medical Image Analysis*, 92:103061, 2024. 2, 3, 7
- [31] Nabil Ibtehaz and Daisuke Kihara. Acc-unet: A completely convolutional unet model for the 2020s. In *International Conference on Medical Image Computing and Computer-Assisted Intervention*, pages 692–702. Springer, 2023. 1, 2, 3
- [32] Fabian Isensee, Paul F Jaeger, Simon AA Kohl, Jens Petersen, and Klaus H Maier-Hein. nnu-net: a self-configuring method for deep learning-based biomedical image segmentation. *Nature methods*, 18(2):203–211, 2021. 1, 5, 6, 7
- [33] Stefan Jaeger, Alexandros Karargyris, Sema Candemir, Les Folio, Jenifer Siegelman, Fiona Callaghan, Zhiyun Xue, Kannappan Palaniappan, Rahul K Singh, Sameer Antani, et al. Automatic tuberculosis screening using chest radiographs. *IEEE transactions on medical imaging*, 33(2):233–245, 2013. 6
- [34] Angelos Katharopoulos, Apoorv Vyas, Nikolaos Pappas, and François Fleuret. Transformers are rnns: Fast autoregressive transformers with linear attention. In *International conference on machine learning*, pages 5156–5165. PMLR, 2020. 2, 3, 4
- [35] Alexander Kirillov, Eric Mintun, Nikhila Ravi, Hanzi Mao, Chloe Rolland, Laura Gustafson, Tete Xiao, Spencer Whitehead, Alexander C Berg, Wan-Yen Lo, et al. Segment anything. In *Proceedings of the IEEE/CVF International Conference on Computer Vision*, pages 4015–4026, 2023. 2, 3, 4, 6, 7
- [36] Bennett Landman, Zhoubing Xu, J Igelsias, Martin Styner, T Langerak, and Arno Klein. Multi-atlas labeling beyond the cranial vault- workshop and challenge. In *International conference on medical image computing and computer-assisted intervention*, 2015. 6, 7
- [37] Chenxin Li, Xinyu Liu, Wuyang Li, Cheng Wang, Hengyu Liu, and Yixuan Yuan. U-kan makes strong backbone for medical image segmentation and generation. *arXiv preprint arXiv:2406.02918*, 2024. 3
- [38] Zihan Li, Yunxiang Li, Qingde Li, Puyang Wang, Dazhou Guo, Le Lu, Dakai Jin, You Zhang, and Qingqi Hong. Lvit: language meets vision transformer in medical image segmentation. *IEEE transactions on medical imaging*, 2023. 3
- [39] Ailiang Lin, Bingzhi Chen, Jiayu Xu, Zheng Zhang, Guangming Lu, and David Zhang. Ds-transunet: Dual swin transformer u-net for medical image segmentation. *IEEE Transactions on Instrumentation and Measurement*, 71:1–15, 2022. 3
- [40] Jiarun Liu, Hao Yang, Hong-Yu Zhou, Yan Xi, Lequan Yu, Yizhou Yu, Yong Liang, Guangming Shi, Shaoting Zhang, Hairong Zheng, et al. Swin-umamba: Mamba-based unet with imagenet-based pretraining. In *International Conference on Medical Image Computing and Computer-Assisted Intervention*, 2024. 3, 5, 6, 7
- [41] Xinyu Liu, Houwen Peng, Ningxin Zheng, Yuqing Yang, Han Hu, and Yixuan Yuan. Efficientvit: Memory efficient vision transformer with cascaded group attention. In *Proceedings of the IEEE/CVF Conference on Computer Vision and Pattern Recognition*, pages 14420–14430, 2023. 4
- [42] Yutong Liu, Haijiang Zhu, Mengting Liu, Huaiyuan Yu, Zihan Chen, and Jie Gao. Rolling-unet: Revitalizing mlp’s ability to efficiently extract long-distance dependencies for medical image segmentation. In *Proceedings of the AAAI Conference on Artificial Intelligence*, pages 3819–3827, 2024. 1, 3, 5, 6, 7
- [43] Jun Ma, Yuting He, Feifei Li, Lin Han, Chenyu You, and Bo Wang. Segment anything in medical images. *Nature Communications*, 15(1):654, 2024. 1, 2, 3, 7
- [44] Maciej A Mazurowski, Haoyu Dong, Hanxue Gu, Jichen Yang, Nicholas Konz, and Yixin Zhang. Segment anything

- model for medical image analysis: an experimental study. *Medical Image Analysis*, 89:102918, 2023. 3
- [45] Ju-Hyeon Nam, Nur Suriza Syazwany, Su Jung Kim, and Sang-Chul Lee. Modality-agnostic domain generalizable medical image segmentation by multi-frequency in multi-scale attention. In *Proceedings of the IEEE/CVF Conference on Computer Vision and Pattern Recognition*, pages 11480–11491, 2024. 2, 3, 5, 6, 7
- [46] José Ignacio Orlando, Huazhu Fu, João Barbosa Breda, Karel Van Keer, Deepti R Bathula, Andrés Diaz-Pinto, Ruogu Fang, Pheng-Ann Heng, Jeyoung Kim, JoonHo Lee, et al. Refuge challenge: A unified framework for evaluating automated methods for glaucoma assessment from fundus photographs. *Medical image analysis*, 59:101570, 2020. 6
- [47] Zhen Qin, Weixuan Sun, Hui Deng, Dongxu Li, Yunshen Wei, Baohong Lv, Junjie Yan, Lingpeng Kong, and Yiran Zhong. cosformer: Rethinking softmax in attention. In *International Conference on Learning Representations*, 2022. 3
- [48] Md Mostafijur Rahman, Mustafa Munir, and Radu Marculescu. Emcad: Efficient multi-scale convolutional attention decoding for medical image segmentation. In *Proceedings of the IEEE/CVF Conference on Computer Vision and Pattern Recognition*, pages 11769–11779, 2024. 2, 5, 6, 7
- [49] Nikhila Ravi, Valentin Gabeur, Yuan-Ting Hu, Ronghang Hu, Chaitanya Ryali, Tengyu Ma, Haitham Khedr, Roman Rädle, Chloe Rolland, Laura Gustafson, et al. Sam 2: Segment anything in images and videos. *arXiv preprint arXiv:2408.00714*, 2024. 2, 7, 8
- [50] Olaf Ronneberger, Philipp Fischer, and Thomas Brox. U-net: Convolutional networks for biomedical image segmentation. In *Medical image computing and computer-assisted intervention—MICCAI 2015: 18th international conference, Munich, Germany, October 5-9, 2015, proceedings, part III 18*, pages 234–241. Springer, 2015. 1, 2, 5, 6, 7, 8
- [51] Jo Schlemper, Ozan Oktay, Michiel Schaap, Mattias Heinrich, Bernhard Kainz, Ben Glocker, and Daniel Rueckert. Attention gated networks: Learning to leverage salient regions in medical images. *Medical image analysis*, 53:197–207, 2019. 2, 5, 6, 7
- [52] Han Shu, Wenshuo Li, Yehui Tang, Yiman Zhang, Yihao Chen, Houqiang Li, Yunhe Wang, and Xinghao Chen. Tinsam: Pushing the envelope for efficient segment anything model. *arXiv preprint arXiv:2312.13789*, 2023. 7
- [53] Ashish Sinha and Jose Dolz. Multi-scale self-guided attention for medical image segmentation. *IEEE journal of biomedical and health informatics*, 25(1):121–130, 2020. 2
- [54] Yanfei Song, Bangzheng Pu, Peng Wang, Hongxu Jiang, Dong Dong, Yongxiang Cao, and Yiqing Shen. Sam-lightening: A lightweight segment anything model with dilated flash attention to achieve 30 times acceleration. *arXiv preprint arXiv:2403.09195*, 2024. 3
- [55] Abhishek Srivastava, Debesh Jha, Sukalpa Chanda, Umada Pal, Håvard D Johansen, Dag Johansen, Michael A Riegler, Sharib Ali, and Pål Halvorsen. Msrf-net: a multi-scale residual fusion network for biomedical image segmentation. *IEEE Journal of Biomedical and Health Informatics*, 26(5):2252–2263, 2021. 3
- [56] Nima Tajbakhsh, Suryakanth R Gurudu, and Jianming Liang. Automated polyp detection in colonoscopy videos using shape and context information. *IEEE transactions on medical imaging*, 35(2):630–644, 2015. 6
- [57] Nikhil Kumar Tomar, Debesh Jha, Michael A Riegler, Håvard D Johansen, Dag Johansen, Jens Rittscher, Pål Halvorsen, and Sharib Ali. Fanet: A feedback attention network for improved biomedical image segmentation. *IEEE Transactions on Neural Networks and Learning Systems*, 34(11):9375–9388, 2022. 1
- [58] Philipp Tschandl, Cliff Rosendahl, and Harald Kittler. The ham10000 dataset, a large collection of multi-source dermatoscopic images of common pigmented skin lesions. *Scientific Data*, 5(1):1–9, 2018. 6, 8
- [59] Jeya Maria Jose Valanarasu and Vishal M Patel. Unext: Mlp-based rapid medical image segmentation network. In *International conference on medical image computing and computer-assisted intervention*, pages 23–33. Springer, 2022. 1, 3, 5, 6, 7
- [60] David Vázquez, Jorge Bernal, F Javier Sánchez, Gloria Fernández-Esparrach, Antonio M López, Adriana Romero, Michal Drozdal, and Aaron Courville. A benchmark for endoluminal scene segmentation of colonoscopy images. *Journal of healthcare engineering*, 2017(1):4037190, 2017. 6, 7
- [61] Ao Wang, Hui Chen, Zijia Lin, Jungong Han, and Guiguang Ding. Repvit-sam: Towards real-time segmenting anything. *arXiv preprint arXiv:2312.05760*, 2023. 8
- [62] Ao Wang, Hui Chen, Zijia Lin, Jungong Han, and Guiguang Ding. Repvit: Revisiting mobile cnn from vit perspective. In *Proceedings of the IEEE/CVF Conference on Computer Vision and Pattern Recognition*, pages 15909–15920, 2024. 4, 6, 7
- [63] Haonan Wang, Peng Cao, Jiaqi Wang, and Osmar R Zaiane. Uctransnet: rethinking the skip connections in u-net from a channel-wise perspective with transformer. In *Proceedings of the AAAI conference on artificial intelligence*, pages 2441–2449, 2022. 1, 3
- [64] Nan Wang, Shaohui Lin, Xiaoxiao Li, Ke Li, Yunhang Shen, Yue Gao, and Lizhuang Ma. Missu: 3d medical image segmentation via self-distilling transunet. *IEEE transactions on medical imaging*, 42(9):2740–2750, 2023. 3
- [65] Ziheng Wang, Xionguo Min, Fangyu Shi, Ruinian Jin, Saida S Nawrin, Ichen Yu, and Ryoichi Nagatomi. Smeswin unet: Merging cnn and transformer for medical image segmentation. In *International Conference on Medical Image Computing and Computer-Assisted Intervention*, pages 517–526. Springer, 2022. 3
- [66] Junde Wu and Min Xu. One-prompt to segment all medical images. In *Proceedings of the IEEE/CVF Conference on Computer Vision and Pattern Recognition*, pages 11302–11312, 2024. 3
- [67] Junde Wu, Wei Ji, Yuanpei Liu, Huazhu Fu, Min Xu, Yanwu Xu, and Yueming Jin. Medical sam adapter: Adapting segment anything model for medical image segmentation. *arXiv preprint arXiv:2304.12620*, 2023. 1, 3, 7

- [68] Kan Wu, Jinnian Zhang, Houwen Peng, Mengchen Liu, Bin Xiao, Jianlong Fu, and Lu Yuan. Tinyvit: Fast pretraining distillation for small vision transformers. In *European conference on computer vision*, pages 68–85. Springer, 2022. 3, 6
- [69] Zhaohu Xing, Tian Ye, Yijun Yang, Guang Liu, and Lei Zhu. Segmamba: Long-range sequential modeling mamba for 3d medical image segmentation. In *International Conference on Medical Image Computing and Computer-Assisted Intervention*, pages 578–588. Springer, 2024. 3, 7
- [70] Yunyang Xiong, Bala Varadarajan, Lemeng Wu, Xiaoyu Xiang, Fanyi Xiao, Chenchen Zhu, Xiaoliang Dai, Dilin Wang, Fei Sun, Forrest Iandola, et al. EfficientSAM: Leveraged masked image pretraining for efficient segment anything. In *Proceedings of the IEEE/CVF Conference on Computer Vision and Pattern Recognition*, pages 16111–16121, 2024. 3, 6, 7, 8
- [71] Jiahao Xu and Lyuyang Tong. Lb-unet: A lightweight boundary-assisted unet for skin lesion segmentation. In *International Conference on Medical Image Computing and Computer-Assisted Intervention*, pages 361–371. Springer, 2024. 1, 3
- [72] Qing Xu, Zhicheng Ma, HE Na, and Wenting Duan. Dcsau-net: A deeper and more compact split-attention u-net for medical image segmentation. *Computers in Biology and Medicine*, 154:106626, 2023. 1, 7
- [73] Xiangyi Yan, Hao Tang, Shanlin Sun, Haoyu Ma, Deying Kong, and Xiaohui Xie. After-unet: Axial fusion transformer unet for medical image segmentation. In *Proceedings of the IEEE/CVF winter conference on applications of computer vision*, pages 3971–3981, 2022. 2
- [74] Moi Hoon Yap, Gerard Pons, Joan Marti, Sergi Ganau, Melcior Sentis, Reyer Zwiggelaar, Adrian K Davison, and Robert Marti. Automated breast ultrasound lesions detection using convolutional neural networks. *IEEE Journal of Biomedical and Health Informatics*, 22(4):1218–1226, 2017. 6
- [75] Weihao Yu and Xinchao Wang. Mambaout: Do we really need mamba for vision? *arXiv preprint arXiv:2405.07992*, 2024. 4
- [76] Weihao Yu, Mi Luo, Pan Zhou, Chenyang Si, Yichen Zhou, Xinchao Wang, Jiashi Feng, and Shuicheng Yan. Metaformer is actually what you need for vision. In *Proceedings of the IEEE/CVF conference on computer vision and pattern recognition*, pages 10819–10829, 2022. 5
- [77] Chaoning Zhang, Dongshen Han, Yu Qiao, Jung Uk Kim, Sung-Ho Bae, Seungkyu Lee, and Choong Seon Hong. Faster segment anything: Towards lightweight sam for mobile applications. *arXiv preprint arXiv:2306.14289*, 2023. 6, 7
- [78] Hong-Yu Zhou, Jiansen Guo, Yinghao Zhang, Xiaoguang Han, Lequan Yu, Liansheng Wang, and Yizhou Yu. nn-former: Volumetric medical image segmentation via a 3d transformer. *IEEE Transactions on Image Processing*, 2023. 2
- [79] Zongwei Zhou, Md Mahfuzur Rahman Siddiquee, Nima Tajbakhsh, and Jianming Liang. Unet++: Redesigning skip connections to exploit multiscale features in image segmentation. *IEEE transactions on medical imaging*, 39(6):1856–1867, 2019. 3, 5, 6, 7
- [80] Lianghai Zhu, Bencheng Liao, Qian Zhang, Xinlong Wang, Wenyu Liu, and Xinggang Wang. Vision mamba: Efficient visual representation learning with bidirectional state space model. In *Forty-first International Conference on Machine Learning*, 2024. 3
- [81] Wenhui Zhu, Xiwen Chen, Peijie Qiu, Mohammad Farazi, Aristeidis Sotiras, Abolfazl Razi, and Yalin Wang. Selfreg-unet: Self-regularized unet for medical image segmentation. In *International Conference on Medical Image Computing and Computer-Assisted Intervention*, pages 601–611. Springer, 2024. 1, 2, 3